Inorganic Chemistry

Article

pubs.acs.org/IC

Subunit Variation to Uncover Properties of Polyazine-Bridged Ru(II), Pt(II) Supramolecules with Low Lying Charge Separated States Providing Insight into the Functioning as H_2O Reduction Photocatalysts to Produce H_2

Jessica D. Knoll, Samantha L. H. Higgins, Travis A. White, and Karen J. Brewer*

Department of Chemistry, Virginia Tech, Blacksburg, Virginia 24061-0212, United States

Supporting Information

ABSTRACT: Two new structurally diverse polyazine-bridged Ru(II),Pt(II) tetrametallic complexes, $[\{(Ph_2phen)_2Ru(dpp)\}_2Ru(dpp)PtCl_2](PF_6)_6$ (**1a**) and $[\{(Ph_2phen)_2Ru(dpp)\}_2Ru(dpq)PtCl_2](PF_6)_6$ (**2a**) (Ph_2phen = 4,7-diphenyl-1,10-phenanthroline, dpp = 2,3-bis(2-pyridyl)pyrazine, dpq = 2,3-bis(2-pyridyl)quinoxaline), as well as their trimetallic precursors have been synthesized to provide a comparison for detailed analysis to elucidate component effects in the previously reported photocatalyst $[\{(phen)_2Ru(dpp)\}_2Ru(dpq)PtCl_2](PF_6)_6$ (**4a**) (phen = 1,10-phenanthroline). Electrochemistry shows terminal Ru based highest occupied molecular orbitals (HOMOs) with remote BL′ (BL′ = bridging ligand coupling central Ru and *cis*-$PtCl_2$ moiety) based lowest unoccupied molecular orbitals (LUMOs). Population of a lowest-lying charge separated (^{3}CS) excited state with oxidized terminal Ru and reduced remote BL′ via intramolecular electron transfer is predicted by electrochemical analysis and is observed through steady-state and time-resolved emission studies as well as emission excitation profiles which display unusual nonunity population of the lowest lying emissive Ru→dpp ^{3}MLCT (metal-to-ligand charge transfer) state. Each tetrametallic complex is an active photocatalyst for H_2 production from H_2O with **2a** showing the highest activity (94 TON (turnover number) in 10 h, where TON = mol H_2/mol catalyst). The nature of the bridging ligand coupling the trimetallic light absorber to the *cis*-$PtCl_2$ moiety has a significant impact on the catalyst activity, correlated to the degree of population of the ^{3}CS excited state. The choice of terminal ligand affects visible light absorption and has a minor influence on photocatalytic H_2 production from H_2O. Evidence that an intact supramolecule functions as the photocatalyst includes a strong dependence of the photocatalysis on the identity of BL′, an insensitivity to Hg(l), no detectable H_2 production from the systems with the trimetallic synthons and *cis*-$[PtCl_2(DMSO)_2]$ as well as spectroscopic analysis of the photocatalytic system.

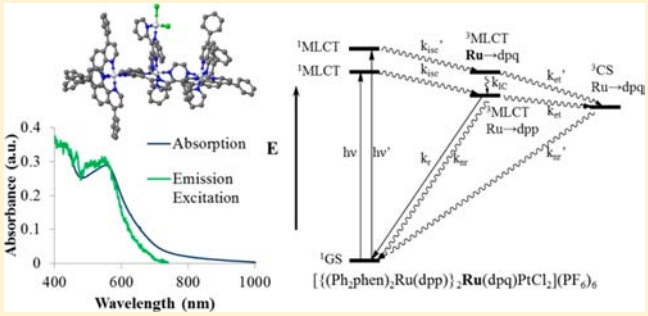

INTRODUCTION

Solar energy conversion via H_2O splitting is an attractive forum in the search for alternative fuel sources as the sun delivers more energy to the surface of the earth in 1 h than the planet consumes in one year.[1] H_2O is a clean, renewable source of H_2, and H_2 fuel has the highest power density of any non-nuclear based fuel.[2−4] Using the sun's energy to split H_2O requires complex, multielectron reactions which occur at the 1.23 V driving force. The half reactions and overall reaction for H_2O splitting are given below for pH = 7 (V vs NHE).[5]

$$4H^+ + 4e^- \rightarrow 2H_2(g) \quad E = -0.41\ V \tag{1}$$

$$2H_2O \rightarrow O_2(g) + 4H^+ + 4e^- \quad E = -0.82\ V \tag{2}$$

$$2H_2O \rightarrow 2H_2(g) + O_2(g) \quad E = -1.23\ V \tag{3}$$

Analogous one electron reactions require about 5 V, energy not available in the solar spectrum. Solar H_2O splitting is a complicated process which requires bond breaking, bond making, and multielectron reactions. While many heterogeneous photocatalysis systems have been reported for each of the half reactions and for H_2O splitting into H_2 and O_2, homogeneous molecular photocatalysts are advantageous as they provide for tunable excited states and systems available to study by electrochemistry and spectroscopy.[6,7] In a general scheme, a successful system for photocatalytic reduction of H_2O to generate H_2 functions through photoexcitation of a chromophore which undergoes inter- or intramolecular electron and/or energy transfer to produce a charge separated state with an appropriate driving force for H_2O reduction, often employing multiple excitations to generate the two electrons needed to produce one molecule of H_2.[8−10]

Received: February 19, 2013
Published: August 13, 2013

   dx.doi.org/10.1021/ic4004406 | *Inorg. Chem.* 2013, 52, 9749−9760

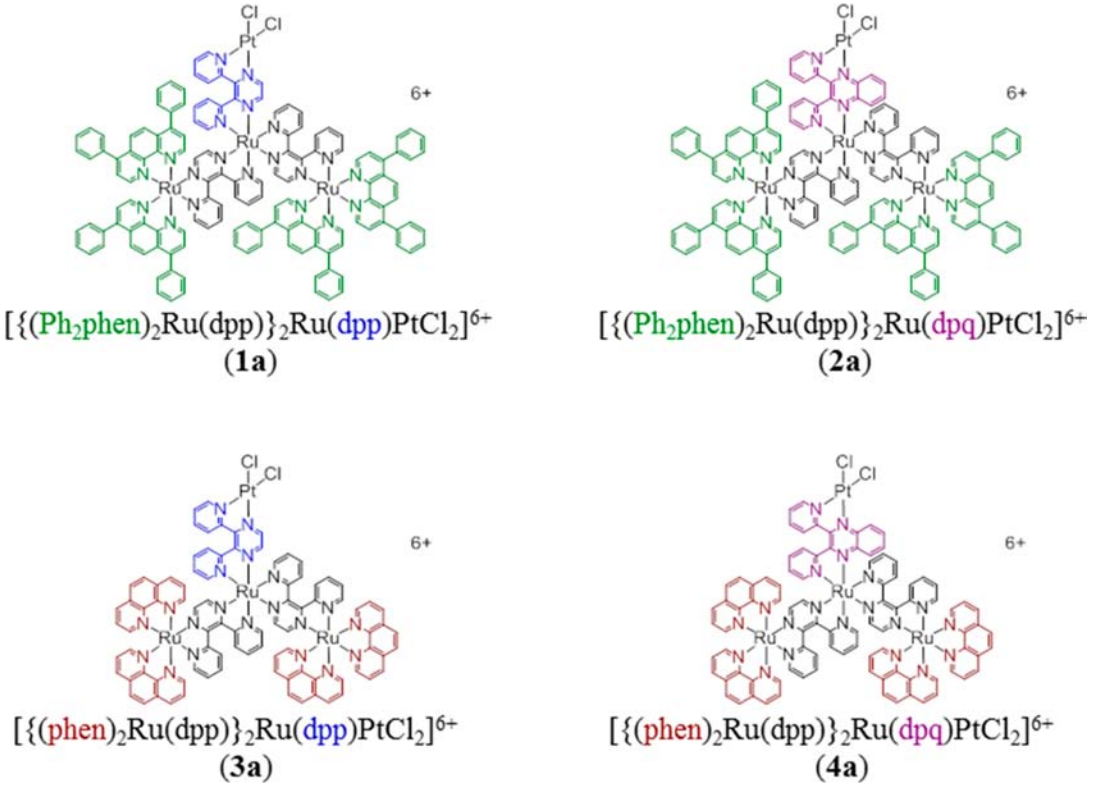

Figure 1. Structural representations of the tetrametallic complexes **1a**, **2a**, **3a**, and **4a**. Ph_2phen = 4,7-diphenyl-1,10-phenanthroline, phen = 1,10-phenanthroline, dpp = 2,3-bis(2-pyridyl)pyrazine, and dpq = 2,3-bis(2-pyridyl)quinoxaline.

Multicomponent photocatalytic H_2O reduction systems have been studied over several decades. One of the first reported multicomponent systems consists of a $[Ru(bpy)_3]^{2+}$ (bpy = 2,2′-bipyridine) light absorber (LA), whose triplet metal-to-ligand charge transfer (^{3}MLCT) excited state possesses the driving force necessary to undergo intermolecular electron transfer to a methyl viologen (MV^{2+}) electron relay.[9] In the presence of a heterogeneous Pt catalyst and H_2O, H_2 gas is evolved. EDTA (ethylenediaminetetraacetic acid) serves as a sacrificial electron donor (ED) by providing reducing equivalents to $[Ru(bpy)_3]^{3+}$ to regenerate $[Ru(bpy)_3]^{2+}$ and impede undesired back electron transfer from $MV^{\bullet+}$ to the oxidized LA. Related systems employ a $[Rh(bpy)_3]^{3+}$ electron relay.[10−12]

Supramolecular complexes covalently couple individual components with specific functions into one molecule to perform a complex function and are known as photochemical molecular devices (PMDs) when that function is induced by light.[13] PMDs are a promising forum to design efficient H_2O reduction photocatalysts.[4,7,14] The components necessary for constructing PMDs for photoinduced H_2O reduction include LA units typically composed of terminal ligands coordinated to a LA metal, bridging ligands to act as electron relays, and a reactive metal center for substrate interaction.[13] Commonly used LAs are Ru(II) polyazine complexes with bidentate polyazine terminal ligands.[15,16] Bis-bidentate polyazine bridging ligands are commonly used to couple Ru-based LAs to reactive metal centers because of their π^* acceptor orbitals which enable electrons to move toward the reactive metal for delivery to a substrate.[17,18] Several reactive metal centers have been coupled to LAs for H_2O reduction photocatalysis, such as Rh,[19−24] Fe,[25] Co,[26,27] Pt,[28−33] and Pd.[34−36] Supramolecular Ru(II),Pt(II), and Ru(II),Pd(II) complexes reported to photocatalytically reduce H_2O to H_2 are few, and their functioning is not well understood. A series of Ru(II),Pt(II) bimetallic complexes which feature a Ru(II) based LA linked to a *cis*-$PtCl_2$ unit through an amidate bridge, $[(bpy)_2Ru(phenNHCO(Rbpy))PtCl_2]^{2+}$ (where phen = 1,10-phenanthroline, R = −COOH or −COOEt) have been reported as active H_2O reduction catalysts in the presence of EDTA, with a quantum yield (Φ) of 0.01 and 5 TON (Turnover Number) in 10 h for R = −COOH,[28,29,31,37] and a dimer of this architecture linked through the Rbpy group was reported to increase efficiency.[38] A bimetallic supramolecular complex $[(^tBu_2bpy)_2Ru(tpphz)PdCl_2]^{2+}$ ($^tBu_2$bpy = 4,4′-di-*tert*-butyl-2,2′-bipyridine, tpphz = tetrapyrido[3,2-*a*:2′,3′-*c*:3″,2″-*h*:2‴,3‴-*j*]phenazine) was reported to produce H_2 with 56 TON in 30 h.[39] The chemical integrity of Ru(II),Pt(II) and Ru(II),Pd(II) complexes upon photolysis has raised controversy as several reports demonstrate colloidal Pt or Pd as the active catalyst.[36,40] Detailed investigations are necessary to understand how each mixed-metal system functions. Systems with a Co reactive metal coupled to Ru LAs produce H_2 from H_2O with $[(bpy)_2Ru(L\text{-}pyr)Co(dmgBF_2)_2(OH_2)]^{2+}$ (L-pyr = [(4-pyridine)oxazolo[4,5-*f*]phenanthroline], $dmgBF_2$ = (difluoroboryl)dimethylglyoximate) affording 56 TON in 4 h when photolyzed in the presence of triethylamine (Et_3N) and $[Et_3NH]^+$.[26]

PMDs that are able to collect multiple electrons in the presence of visible light and an ED are known to undergo photoinitiated electron collection (PEC). PMDs for PEC are of particular interest in H_2O reduction as the less thermodynamically demanding mechanism of H_2O reduction involves multiple electrons; however, few systems are reported. The first reported PMD to undergo PEC was $[\{(bpy)_2Ru$-

dx.doi.org/10.1021/ic4004406 | *Inorg. Chem.* 2013, 52, 9749−9760

$(dpb)\}_2IrCl_2]^{5+}$ (dpb = 2,3-bis(2-pyridyl)benzoquinoxaline) which collects one electron on each of the μ-dpb ligands.[41] Later $[(phen)_2Ru(BL)Ru(phen)_2]^{4+}$ (BL = tatpp = 9,11,20,22-tetraazatetrapyrido[3,2-*a*:2′3′-*c*:3″,2″-*1*:2‴,3‴-*n*]pentacene or tatpq =9,11,20,22-tetraazatetrapyrido[3,2-*a*:2′3′-*c*:3″,2″-*1*:2‴,3‴-*n*]pentacene-10,21-quinone) appeared which collects two and four electrons on the BL π^* orbitals, respectively.[42,43] A monometallic complex $[(bpy)_2Ru(pbn)]^{2+}$ (pbn = 2-(2-pyridyl)benzo[*b*]-1,5-naphthyridine) couples a Ru-based LA to an NAD^+ (nicotinamide adenine dinucleotide) model ligand, which undergoes two proton coupled electron transfers in the presence of Et_3N.[44,45] These complexes, however, are not active photocatalysts for H_2O reduction. The first photoinitiated electron collector reported to act as an active photocatalyst in H_2O reduction, $[\{(bpy)_2Ru(dpp)\}_2RhCl_2]^{5+}$ (dpp = 2,3-bis(2-pyridyl)pyrazine),[20,46] has recently undergone terminal ligand and halide modification to result in the more active complex $[\{(Ph_2phen)_2Ru(dpp)\}_2RhBr_2]^{5+}$ (Ph_2phen = 4,7-diphenyl-1,10-phenanthroline) with Φ = 0.073 and 610 TON in 20 h in the presence of *N*,*N*-dimethylaniline (DMA).[22]

Several supramolecular complexes which couple Ru(II) or Os(II) LAs to a Pt(II) reactive metal through bidentate bridging ligands are reported, yet few systems have been explored as photocatalysts for H_2O reduction. A series of Ru(II),Pt(II) bimetallic complexes with $[(TL)_2M(BL)PtCl_2]^{2+}$ have been reported where M = Ru(II) or Os(II), TL = bpy, phen, and Ph_2phen and BL = dpp, dpq (2,3-bis(2-pyridyl)-quinoxaline), dpb and bpm (2,2′-bipyrimidine).[47−52] Their redox and photophysical properties have been studied, and in some cases their photoinduced interactions with DNA have been studied. The structurally diverse tetrametallic and larger complexes $[Ru\{(dpq)PtCl_2\}_3]^{2+}$,[53] $[Os\{(dpp)Ru[(dpp)-PtCl_2]_2\}_3]^{8+}$,[54] and $[(bpy)_2Os(dpp)Ru\{(dpp)PtCl_2\}_2]^{4+}$,[54] were synthesized and their redox and photophysical properties were investigated. Recently, the redox, spectroscopic, and photophysical properties of a series of complexes of the form $[\{(TL)_2M(dpp)\}_2Ru(BL')PtCl_2]^{6+}$ (M = Ru(II) or Os(II), TL = bpy or phen, BL′ = dpp, dpq, or bpm) were reported,[55,56] and only one of these complexes, $[\{(phen)_2Ru(dpp)\}_2Ru-(dpq)PtCl_2]^{6+}$ (**4a**), has yet been reported to undergo photoreduction and deliver reducing equivalents to a H_2O substrate.[32]

Herein we report the synthesis and electrochemical, spectroscopic, photophysical, and photochemical properties of two new Ru(II),Pt(II) polyazine-bridged tetrametallic complexes $[\{(Ph_2phen)_2Ru(dpp)\}_2Ru(dpp)PtCl_2](PF_6)_6$ (**1a**) and $[\{(Ph_2phen)_2Ru(dpp)\}_2Ru(dpq)PtCl_2](PF_6)_6$ (**2a**) and their trimetallic analogues $[\{(Ph_2phen)_2Ru(dpp)\}_2Ru(dpp)](PF_6)_6$ (**1b**) and $[\{(Ph_2phen)_2Ru(dpp)\}_2Ru(dpq)](PF_6)_6$ (**2b**). The comparison of properties as a function of terminal ligand and BL′ identity provides considerable insight into relative orbital energetics in these supramolecules. The two title Ph_2phen tetrametallic complexes as well as their phen analogues (Figure 1) have been studied as photocatalysts in the visible-light driven reduction of H_2O to produce H_2.

The stabilized dpq-based lowest unoccupied molecular orbital (LUMO) in $[\{(TL)_2Ru(dpp)\}_2Ru(dpq)PtCl_2](PF_6)_6$ (**2a** and **4a**) provides for enhanced driving force for charge separation, a larger driving force for reductive quenching of the excited state, and enhanced H_2 production in comparison with the complexes with BL′ = dpp. Variation of the terminal ligand from phen to Ph_2phen results in fewer spectral gaps, enhancing the visible light absorbing properties of this molecular architecture. The use of Ph_2phen in related Ru,Rh,Ru photocatalysts for H_2 production from H_2O and Ru,Pt complexes as light activated PDT agents provides for enhanced spectral coverage, extended excited state lifetimes, and significant enhancement in reactivity despite the formally Ru→BL ^{3}MLCT and/or Ru→Rh ^{3}MMCT nature of the photoactive states in these complexes.[22,52] These studies prompted the incorporation of Ph_2phen into the title tetrametallic motif. Herein we present the first report of the effect of bridging ligand and terminal ligand variation on this structurally diverse supramolecular architecture through a systematic, detailed study to expand upon preliminary results for the reported photocatalyst $[\{(phen)_2Ru(dpp)\}_2Ru(dpq)-PtCl_2](PF_6)_6$,[32] and uncover the photophysical and photochemical properties imparted by component variation through thorough analysis.

EXPERIMENTAL SECTION

Materials. $[(Ph_2phen)_2RuCl_2]$,[57] $[(Ph_2phen)_2Ru(dpp)](PF_6)_2$,[58] $[\{(phen)_2Ru(dpp)\}_2RuCl_2](PF_6)_4$ (**6**),[32] $[\{(phen)_2Ru(dpp)\}_2Ru-(dpp)](PF_6)_6$ (**3b**),[56] $[\{(phen)_2Ru(dpp)\}_2Ru(dpq)](PF_6)_6$ (**4b**),[32] $[\{(phen)_2Ru(dpp)\}_2Ru(dpp)PtCl_2](PF_6)_6$ (**3a**),[56] $[\{(phen)_2Ru-(dpp)\}_2Ru(dpq)PtCl_2](PF_6)_6$ (**4a**),[32] *cis*-$[PtCl_2(DMSO)_2]$,[59] and dpq[60] were synthesized as previously reported. $AgSO_3CF_3$, Bu_4NCl, and Ph_2phen were purchased from Alfa Aesar. $RuCl_3\cdot 3H_2O$ and Bu_4NPF_6 were received from Fluka. Trifluoromethanesulfonic acid, DMA, dpp, and phen were purchased from Aldrich. NH_4PF_6 and K_2PtCl_4 were purchased from Strem. Solvents were HPLC grade. Spectral grade CH_3CN from Burdick and Jackson was used for electrochemical and spectroscopic studies. All materials were used as received without further purification.

Synthesis of $[\{(Ph_2phen)_2Ru(dpp)\}_2RuCl_2](PF_6)_4$ (5). Two equivalents of the monometallic precursor $[(Ph_2phen)_2Ru(dpp)](PF_6)_2$ (2.0 g, 1.6 mmol) were heated at reflux with $RuCl_3\cdot 3H_2O$ (0.20 g, 0.79 mmol) and excess LiCl (0.50 g, 11 mmol) in 75 mL of EtOH for 24 h. The reaction mixture was cooled to room temperature (RT), and aqueous NH_4PF_6 was added to induce precipitation. The precipitate was collected by vacuum filtration and washed with H_2O and diethyl ether. Purification was achieved by column chromatography with deactivated alumina and a 3:2 toluene/CH_3CN mobile phase. The green band was collected, and the solvent was removed under vacuum. The product was dissolved in 15 mL of CH_3CN and precipitated into 300 mL of diethyl ether, and the precipitate was collected by vacuum filtration. Yield: 1.4 g, 0.51 mmol (65%). ESI-TOF MS: $[M-3PF_6]^{3+}$, m/z = 772.4388.

Synthesis of $[\{(Ph_2phen)_2Ru(dpp)\}_2Ru(dpp)](PF_6)_6$ (1b). The precursor **5** (0.30 g, 0.11 mmol) and 2 equiv of $AgSO_3CF_3$ (0.057 g, 0.22 mmol) were heated at reflux in 20 mL of EtOH for 2 h to remove the chloride ligands. The reaction mixture was then added dropwise to a hot, stirring solution of dpp (0.30 g, 1.3 mmol) in 25 mL of ethylene glycol and heated at reflux for 18 h. The reaction mixture was cooled to RT, and Bu_4NCl (0.10 g, 0.36 mmol) was added to remove Ag^+ as AgCl(s) and aqueous NH_4PF_6 was added to induce precipitation as a PF_6^- salt. The precipitate was collected by vacuum filtration. Purification was achieved on a Sephadex LH-20 size exclusion column with 2:1 EtOH/CH_3CN mobile phase. The major purple-red band was collected, and the solvent removed under vacuum. The product was dissolved in 10 mL of CH_3CN and syringed filtered into 200 mL of diethyl ether to precipitate, and collected by vacuum filtration. Yield: 0.28 g, 0.087 mmol (80%). ESI-TOF MS: $[M-4PF_6]^{4+}$, m/z = 656.2841.

Synthesis of $[\{(Ph_2phen)_2Ru(dpp)\}_2Ru(dpq)](PF_6)_6$ (2b). **2b** was prepared as above by substituting dpq (0.30 g, 0.10 mmol). Yield: 0.35 g, 0.11 mmol (75%). ESI-TOF MS: $[M-4PF_6]^{4+}$, m/z = 669.1125.

Synthesis of $[\{(Ph_2phen)_2Ru(dpp)\}_2Ru(dpp)PtCl_2](PF_6)_6$ (1a). **1b** (0.10 g, 0.031 mmol) and excess *cis*-$[PtCl_2(DMSO)_2]$ (0.10 g, 0.24 mmol) were heated at reflux in 25 mL of methanol for 48 h. The

dx.doi.org/10.1021/ic4004406 | *Inorg. Chem.* 2013, 52, 9749−9760

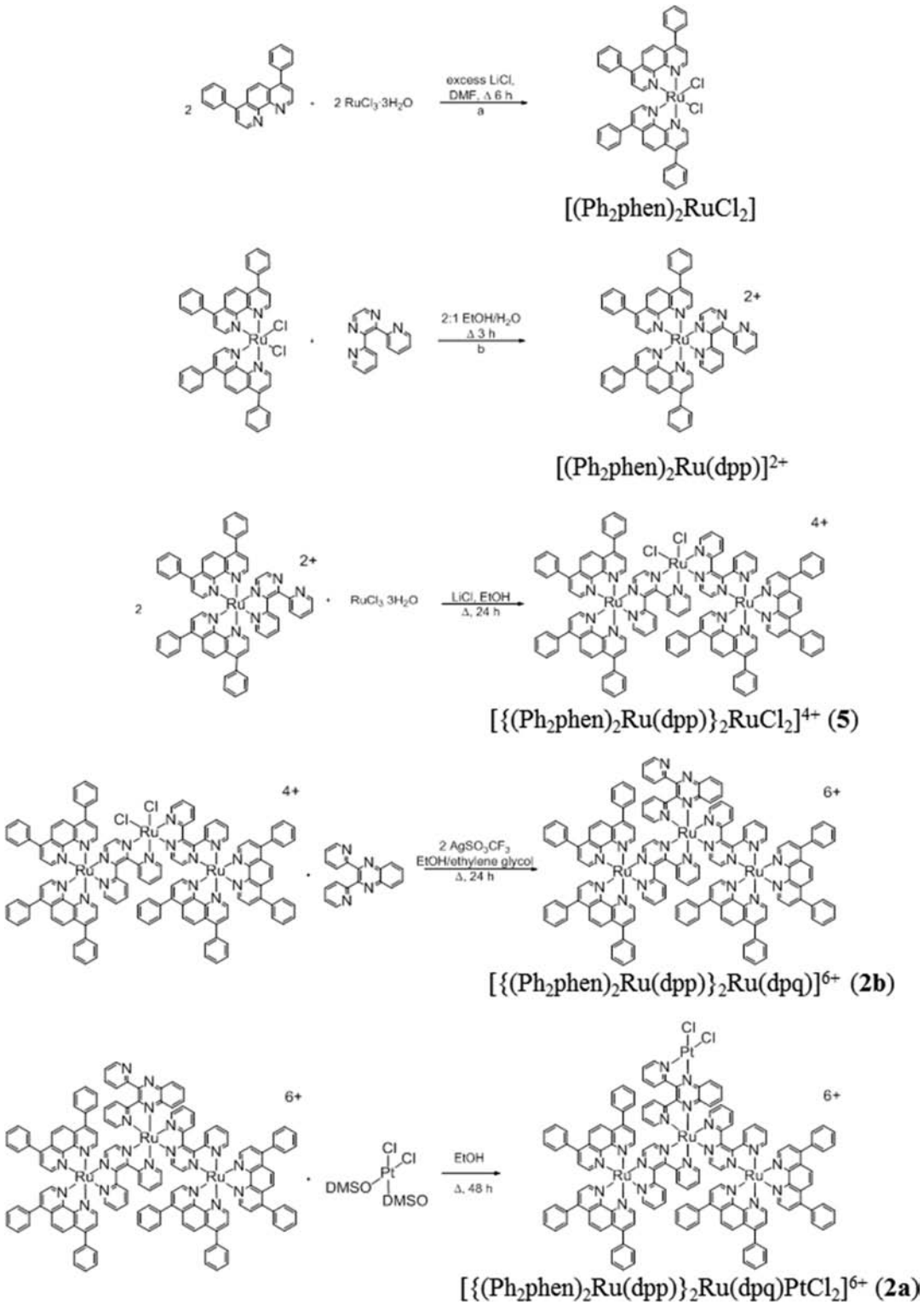

Figure 2. Synthetic scheme for **2a** by the building block method. Ph_2phen = 4,7-diphenyl-1,10-phenanthroline, dpp = 2,3-bis(2-pyridyl)pyrazine, dpq = 2,3-bis(2-pyridyl)quinoxaline. [a] From reference 57. [b] From reference 58.

reaction mixture was cooled to RT and aqueous NH_4PF_6 was added to induce precipitation. The solid was collected by vacuum filtration. Purification was achieved by dissolving in 10 mL of CH_3CN and syringe filtering into 200 mL of diethyl ether several times. Yield: 0.10 g, 0.030 mmol (95%). ESI-TOF MS: $[M-3PF_6]^{3+}$, m/z = 1012.4365.

Synthesis of $[\{(Ph_2phen)_2Ru(dpp)\}_2Ru(dpq)PtCl_2](PF_6)_6$ (2a). **2a** was prepared as above by substituting **2b** (0.10 g, 0.031 mmol). Yield: 0.11 g, 0.030 mmol (95%). ESI-TOF MS: $[M-2PF_6]^{2+}$, m/z = 1616.1486.

ESI-TOF Mass Spectrometry. High resolution mass spectral data were collected by electrospray ionization time-of-flight mass spectrometry performed in CH_3CN with an Agilent Technologies 6220 Accurate-Mass TOF LC-MS (0.4 mL/min flow rate) with a dual ESI source. Low resolution mass spectral analysis of the Pt containing complexes was performed by direct infusion of the sample dissolved in

dx.doi.org/10.1021/ic4004406 | Inorg. Chem. 2013, 52, 9749−9760

CH_3CN (10 μL/min flow rate) into the Thermo Instrument TSQ triple quadrupole mass spectrometer equipped with an ESI source.

Electrochemistry. Cyclic voltammetry and square wave voltammetry were performed in a one compartment, three electrode cell utilizing a glassy carbon working electrode, platinum wire auxiliary electrode, and Ag/AgCl (NaCl, 3 M) reference electrode calibrated against $FeCp_2/FeCp_2^+$ (0.46 V vs Ag/AgCl) with an Epsilon potentiostat from Bioanalytical Systems, Inc. Measurements were recorded at 0.1 V/s in CH_3CN with 0.1 M Bu_4NPF_6 at RT deoxygenated by bubbling with argon. The working electrode was polished with alumina paste prior to analysis.

Electronic Absorption Spectroscopy. Electronic absorption spectroscopy was performed using an Agilent 8453 UV−Vis spectrophotometer with a diode array with 1 nm resolution and a spectral range of 190 to 1100 nm. Spectra were measured in a 1 cm quartz cuvette in CH_3CN at RT. Extinction coefficient experiments were performed in triplicate.

Steady-State, Time-Resolved Emission Spectroscopy, and Emission Excitation Spectroscopy. Steady-state emission spectroscopy and emission excitation spectroscopy were performed on a QuantaMaster Model QM-200-45E fluorometer from Photon Technologies, Inc. (PTI), and spectra were corrected for PMT response. Emission quantum yields were measured vs $[Os(bpy)_3](PF_6)_2$ (Φ^{em} = 0.0046) in deoxygenated RT CH_3CN.[61] Excited state emission lifetime measurements were performed with a PTI PL2300 nitrogen laser pumping a PTI PL 201 continuously tunable dye laser as an excitation source (360−900 nm) with the signal digitized and displayed on a LeCroy 9361 Dual 300 MHz oscilloscope (2.5 Gs/s). RT spectra were measured in deoxygenated CH_3CN, and 77 K spectra were measured in a 4:1 (v/v) EtOH/MeOH glass.

Photochemistry. H_2 production experiments were performed using a locally designed LED array as the light source (λ_{irr} = 470 nm) with a photon flux of 2.3×10^{19} photons/min[62] and H_2 was quantified in real time using HY-OPTIMA 700 in-line process H_2 sensors from H2scan (Valencia, CA).[63] The photocatalyst in a CH_3CN/H_2O solution was injected into an airtight cell with a septum cap and was deoxygenated by bubbling with argon. The ED DMA was separately deoxygenated and injected into the cell just prior to photolysis. The final solution volume was 4.5 mL (50 μM photocatalyst, 0.62 M H_2O, 1.5 M DMA, 0.11 mM $[DMAH^+][CF_3SO_3^-]$) with a headspace volume of about 15.3 mL.

RESULTS AND DISCUSSION

Synthesis and Characterization. The tetrametallic complexes were synthesized by a building block method (Figure 2) which allows for purification and analysis of each precursor. ^1H NMR is not a useful characterization method for such complexes because of the mixture of optical and geometric isomers possible. In supramolecular complexes with several polyazine ligands which possess a large number of C, H, and N atoms, elemental analysis is expected to be too similar between the reported compounds. The precursors and predicted impurities at each step of the synthetic scheme exhibit characteristic redox and spectroscopic properties, providing square wave voltammetry and emission spectroscopy as important tools to assay electrochemical and spectroscopic purity. ESI-MS is used to identify the presence of the high mass product, and the mass spectral data is given in Supporting Information, Table S1. A combination of these diverse methods suggests purity of the complexes. Mixtures of isomers have been reported to have little effect on the spectroscopic properties of Ru(II) polyazine-bridged supramolecular complexes.[64]

Electrochemistry. Cyclic voltammetry and square wave voltammetry of the tetrametallic complexes and their precursors give insight into relative orbital energetics. This is facilitated by our synthetic ability to substitute each subunit of the device, exploring the impact on basic chemical properties. These supramolecules exhibit Ru-based oxidations and ligand-based reductions, with bridging ligand reductions occurring at potentials positive of −1.0 V vs Ag/AgCl. The reductive electrochemistry at potentials more negative than −1.0 V is complex with $BL^{-/2-}$, $TL^{0/-}$, and $TL^{-/2-}$ couples overlapping, so discussion is limited to first bridging ligand reductions. Oxidation and reduction potentials for the new Ph_2phen complexes and their previously reported phen analogues are given in Table 1 with square wave voltammograms of the

Table 1. Electrochemical Data for the Trimetallic and Tetrametallic Complexes with TL = phen and Ph_2phen.[a]

	$E_{1/2}$ (V vs Ag/AgCl)				
complex	oxidation (assignment)[b]		reduction (assignment)[c]		
5	0.86 (**Ru**$^{II/III}$)	1.59 (2Ru$^{II/III}$)	−0.68 (dpp$^{0/-}$)	−0.81 (dpp$^{0/-}$)	
6[d]	0.79 (**Ru**$^{II/III}$)	1.56 (2Ru$^{II/III}$)	−0.70 (dpp$^{0/-}$)	−0.84 (dpp$^{0/-}$)	
1b	1.55 (2Ru$^{II/III}$)		−0.45 (dpp$^{0/-}$)	−0.60 (dpp$^{0/-}$)	−1.02 (**dpp**$^{0/-}$)
2b	1.55 (2Ru$^{II/III}$)		−0.42 (dpp$^{0/-}$)	−0.58 (dpp$^{0/-}$)	−0.79 (**dpq**$^{0/-}$)
3b[e]	1.61 (2Ru$^{II/III}$)		−0.45 (dpp$^{0/-}$)	−0.59 (dpp$^{0/-}$)	−1.00 (**dpp**$^{0/-}$)
4b[d]	1.56 (2Ru$^{II/III}$)		−0.42 (dpp$^{0/-}$)	−0.59 (dpp$^{0/-}$)	−0.80 (**dpq**$^{0/-}$)
1a	1.56 (2Ru$^{II/III}$)		−0.33 (**dpp**$^{0/-}$)	−0.53 (dpp$^{0/-}$)	−0.64 (dpp$^{0/-}$)
2a	1.57 (2Ru$^{II/III}$)		−0.02 (**dpq**$^{0/-}$)	−0.50 (dpp$^{0/-}$)	−0.65 (dpp$^{0/-}$)
3a[e]	1.63 (2Ru$^{II/III}$)		−0.32 (**dpp**$^{0/-}$)	−0.51 (dpp$^{0/-}$)	−0.63 (dpp$^{0/-}$)
4a[d]	1.58 (2Ru$^{II/III}$)		−0.05 (**dpq**$^{0/-}$)	−0.42 (dpp$^{0/-}$)	−0.59 (dpp$^{0/-}$)

[a]Measurements recorded in deoxygenated CH_3CN at RT with 0.1 M Bu_4NPF_6 electrolyte. phen = 1,10-phenanthroline, Ph_2phen = 4,7-diphenyl-1,10-phenanthroline, dpp = 2,3-bis(2-pyridyl)pyrazine, dpq = 2,3-bis(2-pyridyl)quinoxaline. [b]Bold indicates central Ru. [c]Bold indicates BL′. [d]From reference 32. [e]From reference 56.

tetrametallic complexes in Figure 3. For the dichloride trimetallic precursors **6** and **5**, two reversible oxidation couples are observed, with the central $Ru^{II/III}$ oxidation occurring at 0.79 and 0.86 V vs Ag/AgCl for the phen and Ph_2phen complexes, respectively, and at 1.56 and 1.59 V for the two

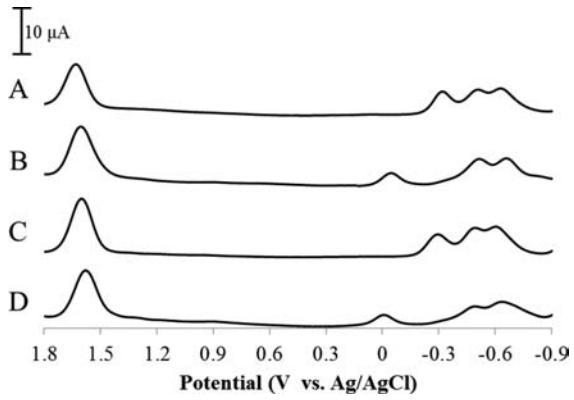

Figure 3. Square wave voltammograms for (A) **3a**, (B) **4a**, (C) **1a**, and (D) **2a** recorded in CH_3CN with 0.1 M Bu_4NPF_6 at RT with potential referenced to Ag/AgCl.

dx.doi.org/10.1021/ic4004406 | Inorg. Chem. 2013, 52, 9749−9760

Table 2. Electronic Absorption Spectroscopy Data[a]

complex	λ_{max}^{abs} (nm)	$\varepsilon \times 10^{-4}$ (M^{-1} cm^{-1})	assignment
5	276	21.3	Ph_2phen $\pi\rightarrow\pi^*$
	315 (sh)	9.1	dpp $\pi\rightarrow\pi^*$
	442	4.5	Ru(dπ)$\rightarrow$$Ph_2phen(\pi^*)$ CT
	625	3.4	Ru(dπ)$\rightarrow$dpp(π^*) CT
6[b]	262	17.2	phen $\pi\rightarrow\pi^*$
	330	5.4	dpp $\pi\rightarrow\pi^*$
	430	2.9	Ru(dπ)$\rightarrow$phen(π^*) CT
	625	3.4	Ru(dπ)$\rightarrow$dpp(π^*) CT
1b	276	19.5	Ph_2phen $\pi\rightarrow\pi^*$
	340 (sh)	5.7	dpp $\pi\rightarrow\pi^*$
	432	4.2	Ru(dπ)$\rightarrow$$Ph_2phen(\pi^*)$ CT
	554	4.2	Ru(dπ)$\rightarrow$dpp(π^*) CT
2b	276	14.4	Ph_2phen $\pi\rightarrow\pi^*$
	340 (sh)	5.5	dpp $\pi\rightarrow\pi^*$, dpq $\pi\rightarrow\pi^*$
	430	3.6	Ru(dπ)$\rightarrow$$Ph_2phen(\pi^*)$ CT
	550	3.6	Ru(dπ)$\rightarrow$dpp(π^*) CT, Ru(dπ)$\rightarrow$dpq(π^*) CT
3b[c]	262	16.6	phen $\pi\rightarrow\pi^*$
	340	4.2	dpp $\pi\rightarrow\pi^*$
	421	2.8	Ru(dπ)$\rightarrow$phen(π^*) CT
	543	3.4	Ru(dπ)$\rightarrow$dpp(π^*) CT
4b[b]	262	15.9	phen $\pi\rightarrow\pi^*$
	350 (sh)	4.8	dpp $\pi\rightarrow\pi^*$, dpq $\pi\rightarrow\pi^*$
	415	2.6	Ru(dπ)$\rightarrow$phen(π^*) CT
	541	3.8	Ru(dπ)$\rightarrow$dpp(π^*) CT, Ru(dπ)$\rightarrow$dpq(π^*) CT
1a	276	17.0	Ph_2phen $\pi\rightarrow\pi^*$
	326 (sh)	7.7	dpp $\pi\rightarrow\pi^*$
	432	4.2	Ru(dπ)$\rightarrow$$Ph_2phen(\pi^*)$ CT
	550	4.2	Ru(dπ)$\rightarrow$dpp(π^*) CT
2a	276	13.9	Ph_2phen $\pi\rightarrow\pi^*$
	340 (sh)	5.2	dpp $\pi\rightarrow\pi^*$, dpq $\pi\rightarrow\pi^*$
	430	3.6	Ru(dπ)$\rightarrow$$Ph_2phen(\pi^*)$ CT
	550	3.1	Ru(dπ)$\rightarrow$dpp(π^*) CT, Ru(dπ)$\rightarrow$dpq(π^*) CT
3a[c]	262	15.5	phen $\pi\rightarrow\pi^*$
	330 (sh)	5.6	dpp $\pi\rightarrow\pi^*$
	421	2.9	Ru(dπ)$\rightarrow$phen(π^*) CT
	543	4.2	Ru(dπ)$\rightarrow$dpp(π^*) CT
4a[b]	262	15.0	phen $\pi\rightarrow\pi^*$
	350 (sh)	4.8	dpp $\pi\rightarrow\pi^*$, dpq $\pi\rightarrow\pi^*$
	415	3.2	Ru(dπ)$\rightarrow$phen(π^*) CT
	541	3.8	Ru(dπ)$\rightarrow$dpp(π^*) CT, Ru(dπ)$\rightarrow$dpq(π^*) CT

[a]Measurements recorded in deoxygenated CH_3CN at RT. phen = 1,10-phenanthroline, Ph_2phen = 4,7-diphenyl-1,10-phenanthroline, dpp = 2,3-bis(2-pyridyl)pyrazine, dpq = 2,3-bis(2-pyridyl)quinoxaline. [b]From reference 32. [c]From reference 56.

overlapping, one electron oxidations of the terminal Ru centers. Coordination of a BL′ in place of the chloride ligands on the central Ru results in stabilization of that Ru center, shifting its oxidation potential outside the solvent window. The trimetallic complexes $[\{(Ph_2phen)_2Ru(dpp)\}_2Ru(BL')](PF_6)_6$ (**1b** and **2b**) possess terminal Ru-based highest occupied molecular orbitals (HOMOs), with an oxidation potential at 1.55 V for both **1b** and **2b**. Replacing Ph_2phen with phen as the terminal ligand results in the terminal $Ru^{II/III}$ oxidation occurring at slightly higher potentials, consistent with the slightly more electron donating nature of Ph_2phen (1.61 and 1.56 V for **3b** and **4b**, respectively). Upon coordination of the *cis*-$PtCl_2$ moiety, the oxidative processes remain similar to the trimetallic precursors and the terminal Ru based HOMO is maintained.

Reductive electrochemistry is predictably complicated. Cathodically, the first reduction of each BL is observed at potentials between 0 V and about −1.0 V vs Ag/AgCl. **5** displays two subsequent one electron reductions at −0.68 and −0.81 V, corresponding to the two μ-dpp ligands, consistent with the previously reported phen analogue **6**. Coordination of the BL′ in place of chlorides results in a shift of the μ-dpp reductions to −0.45 and −0.60 V for **1b** and −0.42 and −0.58 V for **2b**, attributed to the increased positive charge of the complex from +4 to +6 and replacement of σ-donating chloride ligands with a π-accepting BL′. The terminal BL′, prior to coordination to *cis*-$PtCl_2$, is reduced at −1.02 V (**1b**) and −0.79 V (**2b**), consistent with dpq's stabilized acceptor orbitals with respect to dpp. Coordination of the *cis*-$PtCl_2$ unit results in orbital inversion with the LUMO localized on the BL′ between central Ru and Pt, consistent with similar systems which display enhanced stabilization of a polyazine bridging ligand when bound to Pt(II) vs Ru(II).[53] These first reduction processes occur at −0.33 V for **1a** and −0.02 V for **2a**. The two μ-dpp reductions occur following the BL′ reduction. Similar trends are

dx.doi.org/10.1021/ic4004406 | Inorg. Chem. 2013, 52, 9749−9760

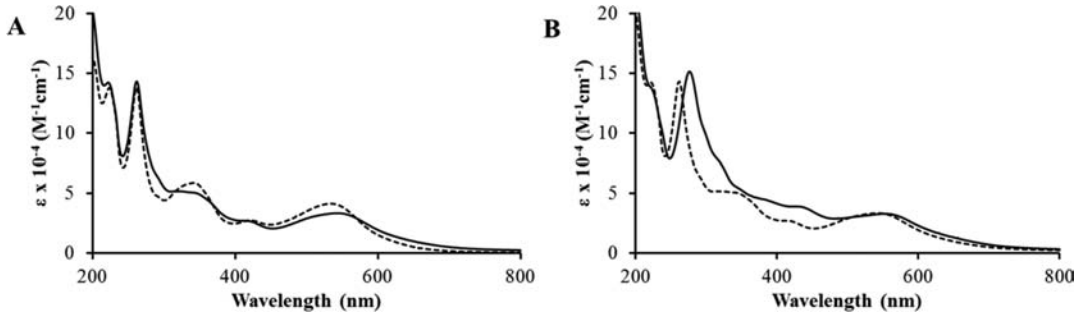

Figure 4. Electronic absorption spectra of (A) **4a** (solid line) and **3a** (dashed line), and (B) **2a** (solid line) and **4a** (dashed line) in CH_3CN at RT.

observed in the TL = phen complexes (**3a** and **4a**). BL′ variation between Ru and Pt has a great impact on the LUMO energy of the tetrametallic complexes, while terminal ligand variation finely tunes the HOMO energy. Relating electrochemical data to HOMO and LUMO localization is particularly valid in the case of the $[\{(TL)_2Ru(dpp)\}_2Ru(BL')](PF_6)_6$ and $[\{(TL)_2Ru(dpp)\}_2Ru(BL')PtCl_2](PF_6)_6$ complexes, as the overall charge of the complex and the HOMO energy level are not impacted upon *cis*-$PtCl_2$ coordination and affect primarily the BL′ acceptor orbitals results in LUMO orbital inversion. The electrochemistry of the tetrametallic complexes suggests a lowest-lying charge separated state upon photoexcitation with an oxidized terminal Ru and reduced remote BL′; the notion of charge separation is important in solar energy conversion schemes.

Electronic Absorption Spectroscopy. The Ph_2phen trimetallic and tetrametallic complexes exhibit electronic absorption spectroscopy trends similar to the previously reported complexes of this molecular architecture; however, the use of Ph_2phen results in enhanced absorptivity throughout the visible region with fewer spectral gaps, typical of Ph_2phen Ru complexes.[65] These complexes are very efficient LAs throughout the UV and visible with ε between $4-20 \times 10^4$ M^{-1} cm^{-1}. The electronic absorption spectroscopy and assignments are summarized in Table 2. The dichloride precursor **5** displays a lowest energy Ru(dπ)→dpp(π^*) CT transition with similar energy and absorptivity to the TL = phen analogue (λ_{max} = 625 nm, $\varepsilon = 3.4 \times 10^4$ M^{-1} cm^{-1}). Utilization of the Ph_2phen terminal ligand results in a molar absorptivity of the Ru(dπ)→Ph_2phen(π^*) CT transition about 440 nm of 4.5×10^4 M^{-1} cm^{-1}, increased vs the molar absorptivity of the Ru(dπ)→phen(π^*) CT transition of 2.9×10^4 M^{-1} cm^{-1} for **6**. The UV region is dominated by Ph_2phen- and dpp-based $\pi \rightarrow \pi^*$ transitions at 276 nm ($\varepsilon = 21.3 \times 10^4$ M^{-1} cm^{-1}) and 315 nm ($\varepsilon = 9.1 \times 10^4$ M^{-1} cm^{-1}), respectively. Replacing the two σ-donating chloride ligands with a π-accepting BL′ (dpp or dpq) stabilizes the central Ru(dπ) orbitals and results in a shift of the lowest energy CT transition (assigned as overlapping Ru(dπ)→dpp(π^*) CT and Ru(dπ)→BL′(π^*) CT transitions) to 554 nm for **1b** and 550 nm for **2b**. These complexes absorb light more efficiently than their TL = phen analogues between 380 and 500 nm because of the enhanced absorptivity of the Ru(dπ)→Ph_2phen(π^*) CT transitions. Coordination of the *cis*-$PtCl_2$ moiety to the trimetallic complexes maintains similar light absorbing properties in the UV and visible regions. In the tetrametallic architecture, variation of BL′ from dpp to dpq results in minor changes to the absorption spectra, while variation of terminal ligand from phen to Ph_2phen enhances the absorptivity between 350 and 500 nm (Figure 4).

Emission Spectroscopy and Photophysics. The excited state processes of the tetrametallic complexes are complicated by the number of energetically close excited states and complex photophysics, resulting in interesting properties. The emissive nature of the lowest lying ^{3}MLCT excited state provides a probe into these processes. Typical of Ru(II) polyazine complexes, population of the ^{1}MLCT excited state leads to intersystem crossing to populate a ^{3}MLCT state with near unit efficiency, and these states are known to undergo intra- and intermolecular electron transfer.[16] The trimetallic models and tetrametallic systems display long-lived Ru→dpp ^{3}MLCT states, much longer than bimetallic systems with directly coupled reactive metals, a design consideration for these complexes.[23,52] Emission spectroscopy for a series of this Ru(II),Pt(II) supramolecular architecture with varied terminal ligand and BL′ was recently reported, and the phen complexes **3a** and **4a** will be discussed in comparison to the Ph_2phen analogues to provide a more detailed analysis of terminal ligand and BL′ effects. The steady-state and time-resolved emission spectroscopy data for the trimetallic and tetrametallic complexes at RT in CH_3CN and at 77 K in a 4:1 EtOH/MeOH rigid matrix are presented in Table 3. The excited state lifetimes for all the trimetallics are quite similar whether the terminal ligand is phen or Ph_2phen, and the same trend is observed for the tetrametallics. This is in contrast to the related Ru,Rh,Ru and Ru,Pt systems where Ph_2phen extends the lifetime of the formally Ru→dpp ^{3}MLCT state.[22,52] The phen analogues were reported to populate the lowest-lying terminal

Table 3. Steady-State and Time-Resolved Emission Spectroscopy Data[a]

	RT						77 K	
complex	λ^{em} (nm)	Φ^{em} x 10^3	τ (μs)	$k_r \times 10^{-3}$ $(s^{-1})^b$	$k_{nr} \times 10^{-6}$ $(s^{-1})^b$	$k_{et} \times 10^{-6}$ (s^{-1})	λ^{em} (nm)	τ (μs)
1b	764	1.04	0.11	9.3	8.9		705	2.0
2b	764	1.09	0.11	9.7	8.9		715	2.0
3b[c]	760	1.01	0.11	9.2	9.1		705	2.1
4b[d]	752	1.01	0.11	9.2	9.1		715	2.0
1a	766	0.71	0.077	9.3	8.9	4.1	715	2.0
2a	760	0.37	0.075	9.7	8.9	4.4	715	2.0
3a[c]	756	0.71	0.083	9.2	9.1	3.0	705	2.1
4a[d]	752	0.32	0.080	9.2	9.1	3.4	715	2.0

[a]Measurements at RT were performed on CH_3CN solutions deoxygenated with Ar. Measurements at 77 K were performed in a 4:1 EtOH/MeOH glass. Values corrected for PMT response. [b]Values for the tetrametallic complexes are assumed to be the same as the values for the corresponding trimetallic complexes. [c]From reference 32. [d]From reference 56.

dx.doi.org/10.1021/ic4004406 | Inorg. Chem. 2013, 52, 9749−9760

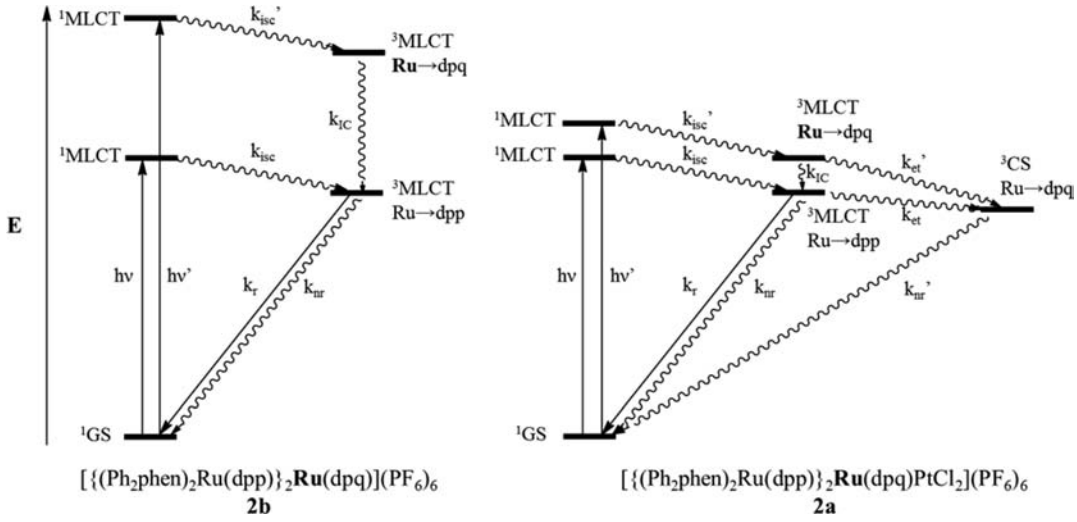

Figure 5. State diagrams for **2b** and **2a**. **Ru** indicates central Ru. Ph_2phen = 4,7-diphenyl-1,10-phenanthroline, dpp = 2,3-bis(2-pyridyl)pyrazine, dpq = 2,3-bis(2-pyridyl)quinoxaline.

Ru(dπ)→dpp(π^*) ^{3}CT excited state with unit efficiency for **3b** and **4b**, but for the tetrametallic complexes **3a** and **4a** a lowest-lying nonemissive ^{3}CS (charge separated) excited state (oxidized terminal Ru and reduced BL′) is competitively populated via intramolecular electron transfer from the emissive terminal Ru(dπ)→dpp(π^*) ^{3}CT state (k_{et}) with some contribution from the higher lying central Ru(dπ)→BL′(π^*) ^{3}CT excited state (k_{et}′). Similar trends are observed for the Ph_2phen analogues and are discussed below. A simplified state diagram for the photophysical processes involved in the trimetallic and tetrametallic complexes is shown in Figure 5.

The state diagrams are greatly simplified to display only the emissive excited state and the state involving BL′ to highlight the effect of Pt coordination on stabilizing the higher lying excited state. The central Ru→μ-dpp CT, terminal Ru→TL CT, and terminal ligand, dpp, and BL′ $\pi\rightarrow\pi^*$ excited states can also be populated; however, they are omitted in the state diagrams as their energies, and subsequent impact on emissive state population, are not expected to significantly change upon Pt coordination. The predicted differences in electronic absorption spectroscopy by primarily lowering the terminal Ru→BL′ CT energy are greatly masked by strong transitions because of multiple Ru→dpp CT and Ru→terminal ligand CT excited states. This results in the expected small shifts in electronic absorption spectroscopy upon *cis*-$PtCl_2$ coordination to BL′.

Both trimetallic complexes **1b** and **2b** emit at 764 nm from the formally terminal Ru(dπ)→dpp(π^*) ^{3}MLCT excited state with Φ^{em} = 1.04 × 10^{-3} and 1.09 × 10^{-3} for **1b** and **2b**, respectively, and both complexes have relatively long-lived excited state lifetimes of 0.11 μs, similar to the values reported for the TL = phen analogues. Upon platination of these trimetallic complexes, the resulting tetrametallic complexes emit at similar energies, yet a quenching of the emission is observed (Φ^{em} = 7.1 × 10^{-4} for **1a** and 3.7 × 10^{-4} for **2a**), as well as a reduction of the excited state lifetime, although to a lesser extent (0.077 μs for **1a** and 0.075 μs for **2a**). While enhanced nonradiative decay upon addition of the *cis*-$PtCl_2$ unit to BL′ may result in the shortened excited state lifetimes, the discrepancy in the degree of quenching of Φ^{em} between BL′ = dpp and dpq is not expected to be influenced only by enhanced nonradiative decay. An important aspect of this molecular architecture is the emission that arises from the part of the molecule that is remote from BL′ and Pt. The unusual discrepancy in the effect on Φ^{em} and τ suggests that another excited state is competitively populated, and this degree of population is strongly influenced by the energy of the BL′ acceptor orbitals. The excited state lifetime is not reduced at 77 K upon platination of the trimetallic to produce the tetrametallic complexes, and the emission profiles are nearly identical, indicating that intramolecular electron transfer observed at RT is impeded in low temperature rigid media.

To study the intramolecular electron transfer to populate the ^{3}CS state from the emissive terminal Ru→dpp ^{3}MLCT excited state (k_{et}) in the tetrametallic complexes, the trimetallic analogues **1b** and **2b** were used as models. These models are particularly valid as they possess the same Ru→μ-dpp ^{3}MLCT emissive state with the dpp coordinated to two Ru centers as the title tetrametallic complex, the excited states are very similar in energy and band shape, the μ-dpp is in the same coordination environment, and the terminal ligands bound to Ru are the same. Equations 4 and 5 give information on k_{et} based on the change in excited state lifetimes (τ).

$$\tau_{model} = \frac{1}{k_r + k_{nr}} \quad (4)$$

$$\tau_{tetrametallic} = \frac{1}{k_r + k_{nr} + k_{et}} \quad (5)$$

The rate constants for radiative and nonradiative decay (k_r and k_{nr}, respectively) are assumed to be the same in the trimetallic models and the tetrametallic analogues; these rate constants and k_{et} are given in Table 3. **4a** and **2a** have larger k_{et} values than their BL′ = dpp (**3a** and **1a**) analogues, indicating more efficient population of the ^{3}CS excited state from the lowest-lying emissive ^{3}MLCT state. This is expected because of the about 0.3 V increased driving force for intramolecular electron transfer in the dpq acceptor systems relative to dpp.

The quantum yields of emission can also be related to the rate constants for the processes deactivating the emissive state with the trimetallic as a model in eqs 6 and 7.

dx.doi.org/10.1021/ic4004406 | *Inorg. Chem.* 2013, 52, 9749−9760

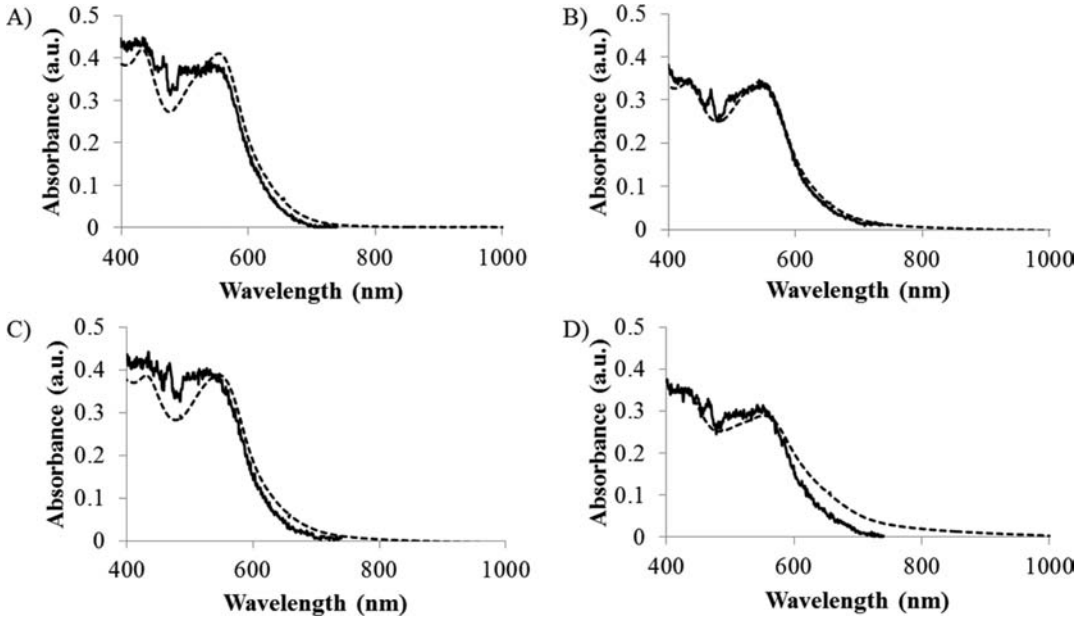

Figure 6. Overlaid absorption (dashed line) and excitation (solid line) spectra of (A) **1b**, (B) **2b**, (C) **1a**, and (D) **2a** in deoxygenated CH_3CN at RT.

$$\Phi_{^3\mathrm{MLCT}}^{\mathrm{em(model)}} = \Phi_{^3\mathrm{MLCT}}^{\mathrm{pop(model)}}\left(\frac{k_r}{k_r + k_{nr}}\right) \quad (6)$$

$$\Phi_{^3\mathrm{MLCT}}^{\mathrm{em(tetrametallic)}} = \Phi_{^3\mathrm{MLCT}}^{\mathrm{pop(tetrametallic)}}\left(\frac{k_r}{k_r + k_{nr} + k_{et}}\right) \quad (7)$$

The tetrametallic complexes display slightly shortened ^{3}MLCT excited state lifetimes but dramatically reduced quantum yields for emission. In eq 6, the quantum yield of population of the lowest-lying ^{3}MLCT state is assumed to be unity, typical of Ru-polyazine complexes.[16] The quantum yield of population of this state in eq 7 is not unity in the tetrametallic architecture, a very unusual property of these systems. This is due to population of the ^{3}CS state from a higher lying state. The Φ^{pop} of the emissive state can be calculated based on the excited state lifetimes and emission quantum yields. The complexes with BL′ = dpp populate the emissive excited state with Φ = 0.93 (**3a**) and 0.99 (**1a**) in line with typical Ru complexes, suggesting minimal indirect population of the nonemissive ^{3}CS state from higher lying ^{3}MLCT states. The BL′ = dpq complexes populate the emissive state with Φ = 0.44 (**4a**) and 0.51 (**2a**), an uncommon property imparted by this tetrametallic motif. This suggests the population of the emissive state would depend on the wavelength of excitation even though these complexes have a variety of MLCT states that are very close in energy. The excitation spectra for the Ph_2phen tetrametallic complexes and model trimetallic systems are provided in Figure 6, illustrating that the excitation spectra follow the absorption profile for the trimetallic systems (**1b** and **2b**) and the BL′ = dpp tetrametallic complexes (**1a**) but vary in the tetrametallics with BL′ = dpq (**2a**). This is in agreement with the unity population of the emissive state in the trimetallics and near unity population of the emissive state when BL′ = dpp and enhanced population of the nonemissive ^{3}CS state resulting in nonunity population of the lowest energy ^{3}MLCT state when BL′ = dpq. These results suggest a higher-lying excited state, likely the central Ru→BL′ CT state, directly populates the ^{3}CS state when BL′ = dpq.

Photochemistry. The tetrametallic complex **4a** was recently reported as an active photocatalyst for H_2O reduction to generate H_2,[32] and herein we report the effects of terminal ligand and BL′ variation on this tetrametallic supramolecular architecture. The four tetrametallic complexes display photocatalysis reducing H_2O to H_2. A system containing 50 μM $[\{(TL)_2Ru(dpp)\}_2Ru(BL')PtCl_2](PF_6)_6$ complex (**1a**–**4a**), 0.62 M H_2O, 1.5 M DMA ED, and 110 μM $[DMAH^+][CF_3SO_3^-]$ irradiated at 470 nm produces H_2 from the H_2O substrate (Figure 7, Table 4). A dramatic difference in photocatalytic activity is observed upon variation of the nature of BL′, with **2a** producing 21 μmol H_2 (94 TON, where TON = mol H_2/mol catalyst) in 10 h compared to the dpp analogue **1a** producing only 5.3 μmol H_2 (23 TON). The same trend is observed for the phen analogues, with **4a** and **3a** producing 15 μmol H_2 (66 TON) and 4.0 μmol H_2 (18 TON), respectively. The $[\{(TL)_2Ru(dpp)\}_2Ru(dpq)PtCl_2](PF_6)_6$ (**2a** and **4a**)

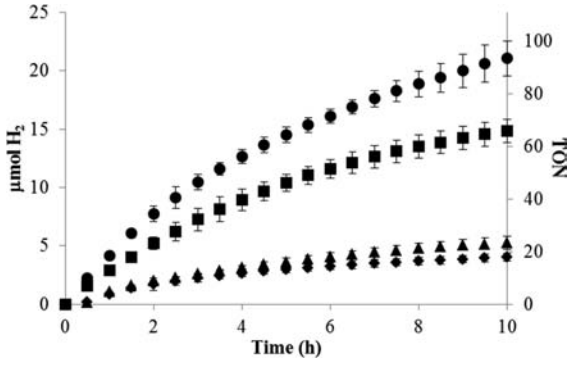

Figure 7. Hydrogen production profiles for photolysis systems with **2a** (circles), **4a** (squares), **1a** (triangles), and **3a** (diamonds). Photolysis systems contained 50 μM tetrametallic complex, 0.62 M H_2O, 1.5 M DMA, and 110 μM $[DMAH^+][CF_3SO_3^-]$ in deoxygenated CH_3CN and irradiated at 470 nm. TON = mol H_2/mol catalyst.

dx.doi.org/10.1021/ic4004406 | Inorg. Chem. 2013, 52, 9749–9760

Table 4. Hydrogen Production Data for Ru(II),Pt(II) Tetrametallic Complexes[a]

complex	μmol H_2 at 10 h	TON at 10 h[b]
1a	5 ± 1	23 ± 2
2a	21 ± 1	94 ± 6
3a	4 ± 1	18 ± 1
4a	15 ± 1	66 ± 4
1b + *cis*-$[PtCl_2(DMSO)_2]$	*c*	
2b + *cis*-$[PtCl_2(DMSO)_2]$	*c*	
3b + *cis*-$[PtCl_2(DMSO)_2]$	*c*	
4b + *cis*-$[PtCl_2(DMSO)_2]$	*c*	

[a]Results correspond to 10 h photolysis time with 470 nm LED light source (light flux = 2.36 × 10^{19} photons/min). Photolysis solutions contained 50 μM tetrametallic complex (or 50 μM trimetallic complex and 50 μM *cis*-$[PtCl_2(DMSO)_2]$), 0.62 M H_2O, 1.5 M DMA, 110 μM $[DMAH^+][CF_3SO_3^-]$ in deoxygenated CH_3CN. [b]TON = mol H_2/mol catalyst. [c]No H_2 detected.

system has a higher driving force for intramolecular electron transfer and a lower lying π^* acceptor orbital on the dpq ligand bound to the catalytically active Pt site which enhances H_2 production. These dpq containing systems also have reduced population of the emissive ^{3}MLCT state, $\Phi^{pop}{}_{^3MLCT}$ = 0.51 for **2a** and 0.44 for **4a**, providing enhanced population of the ^{3}CS state. This suggests an important role in photocatalysis of this ^{3}CS state. The substantially stabilized dpq(π^*) orbital relative to dpp may also impede back electron transfer from BL′ to dpp as this process is substantially uphill in the dpq systems and nearly energy neutral in the dpp systems. The rate constants for emission quenching by the ED DMA (Supporting Information, Figure S7 and Table S2) for the four tetrametallic complexes are in the range of 3.3−5.4 × 10^9 M^{-1} s^{-1}, which is near the diffusion controlled limit. This suggests that upon photoexcitation to populate an MLCT excited state, reductive quenching occurs very rapidly to afford electron collection on the bridging ligands, and from this reduced complex H_2O is reduced to produce H_2.

While the identity of BL′ has a strong impact on the efficiency of the supramolecular architecture in photocatalytic production of H_2 from H_2O, the terminal ligand only serves to fine-tune the activity. This is somewhat surprising as the $[\{(Ph_2phen)_2Ru(dpp)\}_2RhBr_2](PF_6)_5$ system was recently shown by our group to be a far superior photocatalyst than the phen analogue.[22] In addition, the $[(Ph_2phen)_2Ru(dpp)PtCl_2]Cl_2$ system has been shown to provide DNA photocleavage in stark contrast to the lack of activity of bpy and phen analogues.[52] Utilization of Ph_2phen does result in enhanced absorptivity of the photocatalyst throughout the visible range in comparison to the phen analogues. The BL′ dependence strongly supports intact supramolecules as active photocatalysts, as Pt decomplexation would revert the LUMO to the dpp and the lowest lying excited state terminal Ru→dpp ^{3}MLCT, independent of the dpq BL′.

The importance of BL′ in this motif for photocatalysis supports intact supramolecules as being the active photocatalyst which is further supported by additional control experiments described below. Photocatalytic H_2O reduction with **4a** was not impeded by addition of Hg(l), indicating the molecular architecture does not dissociate to form the trimetallic LA **4b** and colloidal Pt.[66] Further evidence for the tetrametallic supramolecular architecture remaining intact during photolysis is provided by experiments in which equimolar amounts of $[\{(TL)_2Ru(dpp)\}_2Ru(BL')](PF_6)_6$ (**1b**−**4b**) and *cis*-$[PtCl_2(DMSO)_2]$ were used in the photolysis system in place of the analogous $[\{(TL)_2Ru(dpp)\}_2Ru(BL')PtCl_2](PF_6)_6$ (**1a**−**4a**). The systems with $[\{(TL)_2Ru(dpp)\}_2Ru(BL')](PF_6)_6$ and *cis*-$[PtCl_2(DMSO)_2]$ produced no detectable H_2 after 10 h photolysis for each combination of terminal ligand and BL′, and in each case, solid precipitate was observed in the bottom of each photolysis cell which indicates in situ formation of Pt^0. Additionally, the electronic absorption spectroscopy after photolysis is noticeably different for each $[\{(TL)_2Ru(dpp)\}_2Ru(BL')PtCl_2](PF_6)_6$ and its analogous $[\{(TL)_2Ru(dpp)\}_2Ru(BL')](PF_6)_6$ and *cis*-$[PtCl_2(DMSO)_2]$ sample (Figure 8), suggesting that the species present in the photolysis samples are different.

CONCLUSIONS

Two new mixed-metal, mixed-ligand complexes of the form $[\{(Ph_2phen)_2Ru(dpp)\}_2Ru(BL')PtCl_2](PF_6)_6$ as well as their trimetallic precursors $[\{(Ph_2phen)_2Ru(dpp)\}_2Ru(BL')](PF_6)_6$, where BL′ = dpp or dpq, were synthesized and their spectroscopy, electrochemistry, photophysics, and photochemistry were studied in comparison to their phen analogues. Detailed analysis of the Ph_2phen systems, **3a**, and the previously explored **4a** are provided, focusing on excited state and photocatalytic properties. Introduction of Ph_2phen into this supramolecular architecture has a minor impact on the orbital energetics of these complexes, while it has a significant impact on the light absorbing properties with highly efficient visible light absorptivity. Interestingly, the Ru→dpp ^{3}MLCT lifetime is not substantially lengthened in this motif unlike the $[\{(Ph_2phen)_2Ru(dpp)\}_2RhBr_2](PF_6)_5$ and $[(Ph_2phen)_2Ru(dpp)PtCl_2]Cl_2$ motifs. Variation of BL′ from dpp to dpq

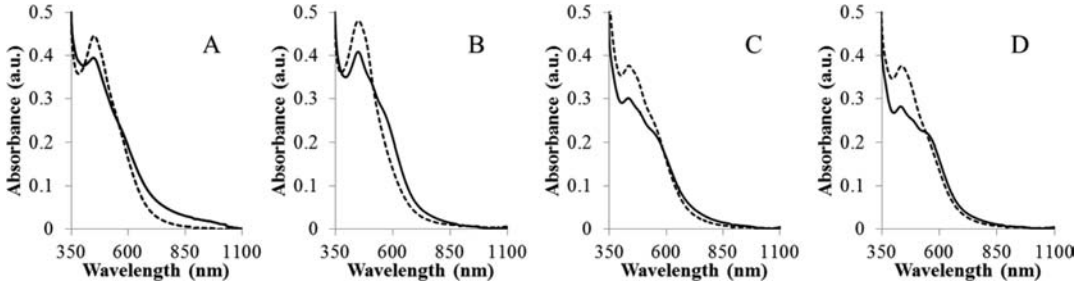

Figure 8. Electronic absorption spectroscopy after 10 h of photolysis in CH_3CN in the presence of 1.5 M DMA, 0.62 M H_2O, 110 μM $[DMAH^+][CF_3SO_3^-]$ and (A) 50 μM **2a** (solid line) or 50 μM **2b** and 50 μM *cis*-$[PtCl_2(DMSO)_2]$ (dashed line), (B) 50 μM **1a** (solid line) or 50 μM **1b** and 50 μM *cis*-$[PtCl_2(DMSO)_2]$ (dashed line), (C) 50 μM **4a** (solid line) or 50 μM **4b** and 50 μM *cis*-$[PtCl_2(DMSO)_2]$ (dashed line), and (D) 50 μM **3a** (solid line) or 50 μM **3b** and 50 μM *cis*-$[PtCl_2(DMSO)_2]$ (dashed line).

dx.doi.org/10.1021/ic4004406 | *Inorg. Chem.* 2013, 52, 9749−9760

results in a more stabilized LUMO and lowest-lying ^{3}CS excited state. A probe into the excited state dynamics of the molecular architecture is provided by population of an emissive ^{3}MLCT excited state. This emissive state is populated with nonunit efficiency as a result of competitive population of the ^{3}CS state with oxidized terminal Ru and reduced BL′, a very unusual property displayed by these systems. The identity of BL′ has the largest impact on Φ^{pop} of the emissive state, with near unity population for $[\{(TL)_2Ru(dpp)\}_2Ru(dpp)PtCl_2](PF_6)_6$ (**1a** and **3a**) and greatly decreased population for $[\{(TL)_2Ru(dpp)\}_2Ru(dpq)PtCl_2](PF_6)_6$ (**2a** and **4a**). Most supramolecular H_2O reduction photocatalysts have very short-lived excited states, making excited state analysis more difficult. The relatively long-lived excited state in this tetrametallic architecture arising from spatial separation of the LA and reactive metal provides a means to deeply study the excited state dynamics to understand the complexes' photoactivity. Enhanced photocatalysis of H_2 production from H_2O is observed for $[\{(TL)_2Ru(dpp)\}_2Ru(dpq)PtCl_2](PF_6)_6$ in comparison to the BL′ = dpp analogue, suggesting that the population of the ^{3}CS excited state is important in this function. Both complexes with Ph_2phen provide slightly enhanced photocatalysis compared to their phen analogues in stark contrast to the dramatically enhanced photocatalysis by $[\{(Ph_2phen)_2Ru(dpp)\}_2RhBr_2](PF_6)_5$ relative to the phen analogue. Evidence supports the functioning of the tetrametallic architecture as the active photocatalyst. Active supramolecular photocatalysis is supported by the Hg test, the large impact of the identity of the BL′ on photocatalyst activity, and the lack of functioning of a $[\{(TL)_2Ru(dpp)\}_2Ru(BL')](PF_6)_6$ (**1**−**4b**) and *cis*-$[Pt(DMSO)_2Cl_2]$ system as well as spectroscopic differences of the supramolecular photocatalyst versus the trimetallic and Pt system. The in depth analysis presented herein is significant as few analyses of Ru,Pt or Ru,Pd supramolecular photocatalysts for H_2O reduction are reported. Further studies into the factors impacting photocatalytic H_2 production from H_2O using these complexes are ongoing.

■ ASSOCIATED CONTENT

Ⓢ Supporting Information

ESI-MS data, steady-state emission spectra, time-resolved emission profiles, and Stern−Volmer emission quenching experiments. This material is available free of charge via the Internet at http://pubs.acs.org.

■ AUTHOR INFORMATION

Corresponding Author

*E-mail: kbrewer@vt.edu.

Notes

The authors declare no competing financial interest.

■ ACKNOWLEDGMENTS

Acknowledgment is made to Hannah Mallalieu for assistance with this manuscript and to the Chemical Sciences, Geosciences and Biosciences Division, Office of Basic Energy Sciences, Office of Sciences, U.S. Department of Energy (DE FG02-05ER15751) for their generous support of the development of new LAs used in this research.

■ ABBREVIATIONS

BL′ = bridging ligand between Ru(II) and Pt(II)
bpm = 2,2′-bipyrimidine
bpy = 2,2′-bipyridine
CS = charge separated state
CT = charge transfer
DMA = *N*,*N*-dimethylaniline
$dmgBF_2$ = (difluoroboryl)dimethylglyoximate
dpb = 2,3-bis(2-pyridyl)benzoquinoxaline
dpp = 2,3-bis(2-pyridyl)pyrazine
dpq = 2,3-bis(2-pyridyl)quinoxaline
ED = sacrificial electron donor
EDTA = ethylenediaminetetraacetic acid
HOMO = highest occupied molecular orbital
k_{et} = rate constant for electron transfer
k_{ic} = rate constant for internal conversion
k_{isc} = rate constant for intersystem crossing
k_{nr} = rate constant for nonradiative decay
k_r = rate constant for radiative decay
LA = light absorber
L-pyr = (4-pyridine)oxazolo-[4,5-*f*]phenanthroline
LUMO = lowest unoccupied molecular orbital
MLCT = metal-to-ligand charge transfer
MMCT = metal-to-metal charge transfer
MV^{2+} = methyl viologen
NAD^+ = nicotinamide adenine dinucleotide
NHE = normal hydrogen electrode
pbn = 2-(2-pyridyl)benzo[*b*]-1,5-naphthyridine
PEC = photoinitiated electron collection
Ph_2phen = 4,7-diphenyl-1,10-phenanthroline
phen = 1,10-phenanthroline
PMD = photochemical molecular device
tatpp = 9,11,20,22-tetraazatetrapyrido[3,2-*a*:2′3′-*c*:3″,2″-*1*:2‴,3‴-*n*]pentacene
tatpq = 9,11,20,22-tetraazatetrapyrido[3,2-*a*:2′3′-*c*:3″,2″-*1*:2‴,3‴-*n*]pentacene-10,21-quinone
$^tBu_2$bpy = 4,4′-di-*tert*-butyl-2,2′-bipyridine
TON = turnover number
tpphz = tetrapyrido[3,2-*a*:2′,3′-*c*:3″,2″-*h*:2‴,3‴-*j*]phenazine
ε = molar absorptivity
τ = lifetime
Φ = quantum yield

■ REFERENCES

(1) Lewis, N. S.; Nocera, D. G. *Proc. Natl. Acad. Sci. U. S. A.* **2006**, *103*, 15729−15735.
(2) Lewis, N. S. *ChemSusChem* **2009**, *2*, 383−386.
(3) Lubitz, W.; Tumas, W. *Chem. Rev.* **2007**, *107*, 3900−3903.
(4) Tinker, L. L.; McDaniel, N. D.; Bernhard, S. *J. Mater. Chem.* **2009**, *19*, 3328−3337.
(5) Bard, A. J.; Fox, M. A. *Acc. Chem. Res.* **1995**, *28*, 141−145.
(6) Esswein, A. J.; Nocera, D. G. *Chem. Rev.* **2007**, *107*, 4022−4047.
(7) Inagaki, A.; Akita, M. *Coord. Chem. Rev.* **2010**, *254*, 1220−1239.
(8) Lehn, J.-M.; Sauvage, J.-P. *Nouv. J. Chim.* **1977**, *1*, 449−451.
(9) Kalyanasundaram, K.; Kiwi, J.; Grätzel, M. *Helv. Chim. Acta* **1978**, *61*, 2720−2730.
(10) Kirch, M.; Lehn, J.-M.; Sauvage, J.-P. *Helv. Chim. Acta* **1979**, *62*, 1345−1384.
(11) Brown, G. M.; Chan, S. F.; Creutz, C.; Schwarz, H. A.; Sutin, N. *J. Am. Chem. Soc.* **1979**, *101*, 7638−7640.
(12) Chan, S.-F.; Chou, M.; Creutz, C.; Matsubara, T.; Sutin, N. *J. Am. Chem. Soc.* **1981**, *103*, 369−379.
(13) Balzani, V.; Moggi, L.; Scandola, F. In *Supramolecular Photochemistry*; Balzani, V., Ed.; NATO Advanced Study Institute Series 214; Reidel: Dordrecht, The Netherlands, 1987; p 1, and references cited therein.
(14) Wang, M.; Na, Y.; Gorlov, M.; Sun, L. *Dalton Trans.* **2009**, 6458−6467.

(15) Durham, B.; Caspar, J. V.; Nagle, J. K.; Meyer, T. J. *J. Am. Chem. Soc.* **1982**, *104*, 4803−4810.
(16) Kalyanasundaram, K. *Coord. Chem. Rev.* **1982**, *46*, 159−244.
(17) Wallace, A. W.; Murphy, W. R., Jr.; Petersen, J. D. *Inorg. Chim. Acta* **1989**, *166*, 47−54.
(18) Berger, R. M. *Inorg. Chem.* **1990**, *29*, 1920−1924.
(19) Arachchige, S. M.; Brown, J. R.; Chang, E.; Jain, A.; Zigler, D. F.; Rangan, K.; Brewer, K. J. *Inorg. Chem.* **2009**, *48*, 1989−2000.
(20) Elvington, M.; Brown, J.; Arachchige, S. M.; Brewer, K. J. *J. Am. Chem. Soc.* **2007**, *129*, 10644−10645.
(21) Rangan, K.; Arachchige, S. M.; Brown, J.; Brewer, K. J. *Energy Environ. Sci.* **2009**, *2*, 410−419.
(22) White, T. A.; Higgins, S. L. H.; Arachchige, S. M.; Brewer, K. J. *Angew. Chem., Int. Ed.* **2011**, *50*, 12209−12213.
(23) White, T. A.; Whitaker, B. N.; Brewer, K. J. *J. Am. Chem. Soc.* **2011**, *133*, 15332−15334.
(24) Miyake, Y.; Nakajima, K.; Sasaki, K.; Saito, R.; Nakanishi, H.; Nishibayashi, Y. *Organometallics* **2009**, *28*, 5240−5243.
(25) Li, X.; Wang, M.; Zhang, S.; Pan, J.; Na, Y.; Liu, J.; Akermark, B.; Sun, L. *J. Phys. Chem. B* **2008**, *112*, 8198−8202.
(26) Fihri, A.; Artero, V.; Razavet, M.; Baffert, C.; Leibl, W.; Fontecave, M. *Angew. Chem., Int. Ed.* **2008**, *47*, 564−567.
(27) Li, C.; Wang, M.; Pan, J.; Zhang, P.; Zhang, R.; Sun, L. *J. Organomet. Chem.* **2009**, *694*, 2814−2819.
(28) Sakai, K.; Ozawa, H. *Coord. Chem. Rev.* **2007**, *251*, 2753−2766.
(29) Ozawa, H.; Sakai, K. *Chem. Commun.* **2011**, *47*, 2227−2242.
(30) Ozawa, H.; Haga, M.-a.; Sakai, K. *J. Am. Chem. Soc.* **2006**, *128*, 4926−4927.
(31) Masaoka, S.; Mukawa, Y.; Sakai, K. *Dalton Trans.* **2010**, *39*, 5868−5876.
(32) Knoll, J. D.; Arachchige, S. M.; Brewer, K. J. *ChemSusChem* **2011**, *4*, 252−261.
(33) Hirahara, M.; Masaoka, S.; Sakai, K. *Dalton Trans.* **2011**, *40*, 3967−3978.
(34) Singh Bindra, G.; Schulz, M.; Paul, A.; Soman, S.; Groarke, R.; Inglis, J.; Pryce, M. T.; Browne, W. R.; Rau, S.; Maclean, B. J.; Vos, J. G. *Dalton Trans.* **2011**, *40*, 10812−10814.
(35) Karnahl, M.; Kuhnt, C.; Ma, F.; Yartsev, A.; Schmitt, M.; Dietzek, B.; Rau, S.; Popp, J. *ChemPhysChem* **2011**, *12*, 2101−2109.
(36) Lei, P.; Hedlund, M.; Lomoth, R.; Rensmo, H.; Johansson, O.; Hammarström, L. *J. Am. Chem. Soc.* **2008**, *130*, 26−27.
(37) Ozawa, H.; Sakai, K. *Chem. Lett.* **2007**, 36.
(38) Ozawa, H.; Kobayashi, M.; Balan, B.; Masaoka, S.; Sakai, K. *Chem.—Asian J.* **2010**, *5*, 1860−1869.
(39) Rau, S.; Schäfer, B.; Gleich, D.; Anders, E.; Rudolph, M.; Friedrich, M.; Görls, H.; Henry, W.; Vos, J. G. *Angew. Chem., Int. Ed.* **2006**, *45*, 6215−6218.
(40) Du, P.; Schneider, J.; Li, F.; Zhao, W.; Patel, U.; Castellano, F. N.; Eisenberg, R. *J. Am. Chem. Soc.* **2008**, *130*, 5056−5058.
(41) Molnar, S. M.; Nallas, G. N. A.; Bridgewater, J. S.; Brewer, K. J. *J. Am. Chem. Soc.* **1994**, *116*, 5206−5210.
(42) Kim, M.-J.; Konduri, R.; Ye, H.; MacDonnell, F. M.; Puntoriero, F.; Serroni, S.; Campagna, S.; Holder, T.; Kinsel, G.; Rajeshwar, K. *Inorg. Chem.* **2002**, *41*, 2471−2476.
(43) Konduri, R.; Ye, H.; MacDonnell, F. M.; Serroni, S.; Campagna, S.; Rajeshwar, K. *Angew. Chem., Int. Ed.* **2002**, *41*, 3185−3187.
(44) Fukushima, T.; Fujita, E.; Muckerman, J. T.; Polyansky, D. E.; Wada, T.; Tanaka, K. *Inorg. Chem.* **2009**, *48*, 11510−11512.
(45) Polyansky, D. E.; Cabelli, D.; Muckerman, J. T.; Fukushima, T.; Tanaka, K.; Fujita, E. *Inorg. Chem.* **2008**, *47*, 3958−3968.
(46) Elvington, M.; Brewer, K. J. *Inorg. Chem.* **2006**, *45*, 5242−5244.
(47) Sahai, R.; Rillema, D. P. *Inorg. Chim. Acta* **1986**, *118*, L35−L37.
(48) Yam, V. W.-W.; Lee, V. W.-M.; Cheung, K.-K. *J. Chem. Soc., Chem. Commun.* **1994**, 2075−2076.
(49) Milkevitch, M.; Shirley, B. W.; Brewer, K. J. *Inorg. Chim. Acta* **1997**, *264*, 249−256.
(50) Milkevitch, M.; Storrie, H.; Brauns, E.; Brewer, K. J.; Shirley, B. W. *Inorg. Chem.* **1997**, *36*, 4534−4538.
(51) Swavey, S.; Fang, Z.; Brewer, K. J. *Inorg. Chem.* **2002**, *41*, 2598−2607.
(52) Higgins, S. L. H.; White, T. A.; Winkel, B. S. J.; Brewer, K. J. *Inorg. Chem.* **2010**, *50*, 463−470.
(53) Sahai, R.; Rillema, D. P. *J. Chem. Soc., Chem. Commun.* **1986**, 1133−1134.
(54) Sommovigo, M.; Denti, G.; Serroni, S.; Campagna, S.; Mingazzini, C.; Mariotti, C.; Juris, A. *Inorg. Chem.* **2001**, *40*, 3318−3323.
(55) Miao, R.; Mongelli, M. T.; Zigler, D. F.; Winkel, B. S. J.; Brewer, K. J. *Inorg. Chem.* **2006**, *45*, 10413−10415.
(56) Knoll, J. D.; Arachchige, S. M.; Wang, G.; Rangan, K.; Miao, R.; Higgins, S. L. H.; Okyere, B.; Zhao, M.; Croasdale, P.; Magruder, K.; Sinclair, B.; Wall, C.; Brewer, K. J. *Inorg. Chem.* **2011**, *50*, 8850−8860.
(57) Basile, L. A.; Barton, J. K. *J. Am. Chem. Soc.* **1987**, *109*, 7548−7550.
(58) Mongelli, M. T.; Brewer, K. J. *Inorg. Chem. Commun.* **2006**, *9*, 877−881.
(59) Price, J. H.; Williamson, A. N.; Schramm, R. F.; Wayland, B. B. *Inorg. Chem.* **1972**, *11*, 1280−1284.
(60) Goodwin, H. A.; Lions, F. *J. Am. Chem. Soc.* **1959**, *81*, 6415−6422.
(61) Caspar, J. V.; Kober, E. M.; Sullivan, B. P.; Meyer, T. J. *J. Am. Chem. Soc.* **1982**, *104*, 630−632.
(62) Brown, J. R.; Elvington, M.; Mongelli, M. T.; Zigler, D. F.; Brewer, K. J. *Proc. SPIE - Optics and Photonics Solar Hydrogen Nanotechnology*; Lionel, V., Ed.; SPIE: Bellingham, WA, 2006; Vol. *6340*, p 634017.
(63) Arachchige, S. M.; Shaw, R.; White, T. A.; Shenoy, V.; Tsui, H.-M.; Brewer, K. J. *ChemSusChem* **2011**, *4*, 514−518.
(64) MacDonnell, F. M.; Bodige, S. *Inorg. Chem.* **1996**, *35*, 5758−5759.
(65) Crosby, G. A.; Watts, R. J. *J. Am. Chem. Soc.* **1971**, *93*, 3184−3188.
(66) Whitesides, G. M.; Hackett, M.; Brainard, R. L.; Lavalleye, J. P. P. M.; Sowinski, A. F.; Izumi, A. N.; Moore, S. S.; Brown, D. W.; Staudt, E. M. *Organometallics* **1985**, *4*, 1819−1830.